J. Fluid Mech. (1999), *vol.* 383, *pp.* 327–352. Printed in the United Kingdom

Oscillatory flow in a tube of time-dependent curvature. Part 1. Perturbation to flow in a stationary curved tube

By S. L. WATERS AND T. J. PEDLEY

Department of Applied Mathematics and Theoretical Physics, University of Cambridge, Silver Street, Cambridge, CB3 9EW, UK

(Received 26 January 1998 and in revised form 13 October 1998)

Motivated by the study of blood flow in the coronary arteries, this paper examines the flow of an incompressible Newtonian fluid in a tube of time-dependent curvature. The flow is driven by an oscillatory pressure gradient with the same dimensionless frequency, α, as the curvature variation. The dimensionless governing parameters of the flow are α, the curvature ratio δ_0, a secondary streaming Reynolds number R_s and a parameter R_t representing the time-dependence of curvature. We consider the parameter regime $\delta_0 \ll R_t \ll 1$ (R_s and α remain $O(1)$ initially) in which the effect of introducing time-dependent curvature is to perturb the flow driven by an oscillatory pressure gradient in a fixed curved tube. Flows driven by low- and high-frequency pressure gradients are then considered. At low frequency ($\delta_0 \ll R_t \ll \alpha \ll 1$) the flow is determined by using a sequence of power series expansions ($R_s = O(1)$). At high frequency ($\delta_0 \ll R_t \ll 1/\alpha^2 \ll 1$) the solution is obtained using matched asymptotic expansions for the region near the wall (Stokes layer) and the region away from the wall in the interior of the pipe. The behaviour of the flow in the interior is then determined at both small and intermediate values of R_s. For both the low and high frequency cases, we find the principal corrections introduced by the time-varying curvature to the primary and secondary flows, and hence to the wall shear stress. The physiological application to flow in the coronary arteries is discussed.

1. Introduction

The main application of the study of unsteady viscous flows in tubes of time-dependent curvature is to blood flow in the coronary arteries. By far the most common arterial disease is atherosclerosis, and in the coronary arteries alone it is the cause of one third of all deaths in Western society. It has been found that atherosclerotic plaques are distributed at preferential sites on the artery walls, such as at the outer wall of an arterial bifurcation, the inside of curves, and regions where the arterial cross-section undergoes an expansion. The sites at which early atherosclerotic plaques are found, and their subsequent development, are now widely believed to be correlated with the distribution of mean arterial wall shear stress and with its pulsatility (Ku *et al.* 1985; Giddens, Zarins & Glagov 1993; Friedman 1993). It has been observed that plaques tend to develop in regions of low mean wall shear stress and regions where the shear stress changes direction in the course in the cardiac cycle (Caro, FitzGerald & Schroter 1971). Such regions are sites of increased residence time for circulating vasoactive and toxic materials. Thus one mechanism for atherogenesis

is that the endothelium at these sites is exposed to increased contact with atherogenic agents compared to sites where the wall shear stress is elevated or unidirectional.

We consider the extramyocardial coronary arteries that lie on the surface of the beating heart. As the heart beats they experience both a rotation and a translation. Moreover, their overall geometry, represented by the curvature and torsion of the vessel centreline, as well as their diameter and length, changes with time. In this paper we concentrate on variations in the vessel curvature. The flow of blood in the arteries is pulsatile and as a step towards understanding the properties of unsteady flow in a time-dependent curved tube, we shall examine flows driven by oscillatory pressure gradients.

Considerable theoretical attention has been given to fully developed unsteady flow in fixed uniform curved tubes, of small curvature, driven by a time-dependent pressure gradient. The pioneering analytical study by Lyne (1971) considered a sinusoidally oscillating pressure gradient, of period T, with zero mean. At large values of α $(= a(\nu T)^{-1/2}$, where a is the tube radius), Lyne developed a solution by the use of two matched asymptotic expansions. The flow consists of an inviscid core surrounded by a viscous Stokes boundary layer and the Stokes layer thickness, $(\nu T)^{1/2}$, is small compared with the tube radius a. Within the Stokes layer a secondary velocity is generated by the nonlinear 'centrifugal' force terms in the equations. These secondary motions have a non-zero mean which does not fall to zero at the edge of the Stokes layer but instead drives a (two-vortex) steady secondary streaming in the core. The details of this streaming are dependent upon a secondary streaming Reynolds number R_s, but for all values of R_s the direction of the streaming is across the centreline of the tube from the outside of the bend to the inside, the opposite sense to that for steady flow in a curved tube (Dean 1927, 1928).

Mullin & Greated (1980*a*,*b*) also analysed oscillatory developing and fully developed flow in a curved tube. They found an analytical solution to the governing equations when α is assumed to be small, corresponding to the case of a low-frequency driving pressure gradient. The leading-order axial and secondary flow is quasi-steady Dean flow.

Subsequent workers have superimposed a mean onto the oscillatory driving pressure gradient in order to investigate how the two types of secondary motion interact (Smith 1975; Blennerhassett 1976). Blennerhassett also found non-uniqueness at certain parameter values. Numerical and experimental analysis of periodic flow in a curved tube has also been carried out by Lin & Tarbell (1980), Rabadi, Simon & Chow (1980); Hamakiotes & Berger (1990) and Zalosh & Nelson (1973). Quantitative studies of pulsatile entry flow in a curved pipe using flow visualization and hot-film anemometry were reported by Chandran, Yearwood & Wieting (1979) as well as Chandran & Yearwood (1981) and later using laser Doppler anemometry by Talbot & Gong (1983).

Non-fully developed steady and unsteady flow has been examined, both in the forms of entry flow with a flat profile (Singh 1974; Yao & Berger 1975), and of flow entering from a straight pipe with a parabolic profile (Smith 1976).

For more detailed reviews and an explanation of further curved tube flows see Pedley (1980) and Berger, Talbot & Yao (1983).

The problem of flow in a tube with time-dependent curvature was first addressed by Lynch, Waters & Pedley (1996). In that paper, the governing equations are derived from the Navier–Stokes and continuity equations using a coordinate system fixed in the frame of reference of the tube. The tube is assumed to be circular in cross-section with a uniform radius that is independent of time. The centreline of the tube is

assumed to be inextensible and points on the tube wall which at one instant lie in a plane perpendicular to the centreline at a point S_0 remain in that plane as S_0 moves and the plane rotates. The centreline is also assumed to lie in a constant plane (so the torsion is zero). The blood itself is modelled as an incompressible homogeneous viscous Newtonian fluid. The flows driven by a steady pressure gradient in (i) a tube of uniform but time-dependent curvature; and (ii) a sinuous tube, representing a small oscillation from a straight pipe, were analysed by asymptotic methods.

Here we consider fully developed flow driven by an oscillatory pressure gradient in a tube of uniform time-dependent curvature, as a model for those extramyocardial coronary arteries whose curvature is single signed and varies relatively slowly with longitudinal position. The frequency of the pressure gradient oscillation is taken to be the same as that of the curvature, corresponding to the haemodynamic application; both low and high frequencies will be considered. The mean curvature, equal to the ratio of the pipe radius to the mean radius of curvature of the pipe, is δ_0. In § 2.1 we state the dimensionless governing equations. In § 2.2 we derive two secondary streaming Reynolds numbers, R_s and R_{s_1}, which govern the secondary flow behaviour. Although these Reynolds numbers are applicable at both small and large values of α, their derivation is most clearly achieved by assuming α to be large. From R_s and R_{s_1} we define a further parameter R_t which, along with δ_0, R_s and α, is an independent governing parameter of the flow. In order that analytical progress can be made, the many governing parameters are taken to be large or small. Thus there exist numerous different cases for which asymptotic solutions to the governing equations may be sought. In § 2.3 we consider one particular parameter regime in which the secondary flow consists of a small perturbation to that in a fixed curved tube. (See Waters (1996) for a parameter regime in which the secondary motions are driven by the oscillatory rotation and are almost the same as if the pipe were straight.) In § 3 we determine the leading-order governing equations for the chosen parameter regime. In § 4 we consider the flow at low frequency (R_s remains $O(1)$). In § 5 we examine the high frequency case and determine the behaviour of the flow at both small and intermediate values of R_s. We are particularly interested in the secondary flow, especially the non-zero mean part (steady streaming), and its influence on the axial flow. In both §§ 4 and 5 the effect of the time-varying curvature upon the secondary streaming and, consequently, on the axial flow is determined. The magnitude and distribution of the resulting wall shear stress is then found. Finally, in § 6 we briefly discuss the application of this work to flow in the coronary arteries.

2. Governing equations and parameters

2.1. *Full equations*

The governing equations for the pressure-driven flow in a tube of time-dependent curvature are derived in the paper by Lynch *et al.* (1996). Here we give a brief outline of their derivation.

The equations are determined from first principles using the Navier–Stokes and continuity equations for an incompressible viscous fluid:

$$\nabla \cdot \hat{\boldsymbol{u}}' = 0, \tag{2.1a}$$

$$\left.\frac{\partial \hat{\boldsymbol{u}}'}{\partial \hat{t}}\right|_I + (\hat{\boldsymbol{u}}' \cdot \nabla)\,\hat{\boldsymbol{u}}' = -\frac{1}{\rho}\nabla \hat{p} + \nu \nabla^2 \hat{\boldsymbol{u}}'. \tag{2.1b}$$

These equations have been written with respect to an inertial frame of reference

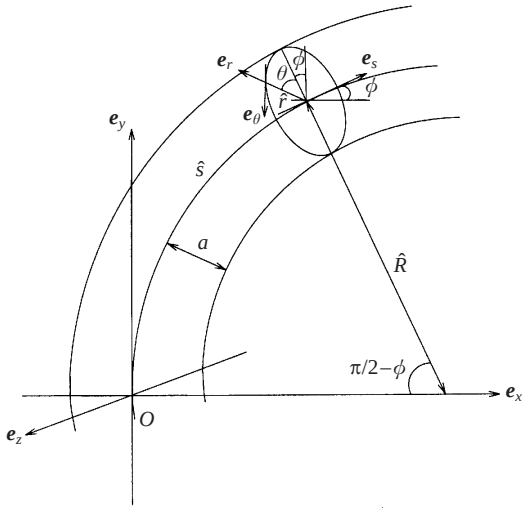

FIGURE 1. The curvilinear coordinate system.

$(\hat{x}, \hat{y}, \hat{z})$; $(\boldsymbol{e}_x, \boldsymbol{e}_y, \boldsymbol{e}_z)$ denote the Cartesian coordinate directions, $\hat{\boldsymbol{u}}'$ is the dimensional velocity vector in this frame, $\hat{p}$ is the dimensional pressure and $\hat{t}$ is the dimensional time; ρ denotes the density and ν the kinematic viscosity of the fluid. We are considering the flow in a tube that is both rotating and translating. A non-inertial, curvilinear coordinate system, $(\hat{r}, \theta, \hat{s})$, is chosen that moves and deforms with the pipe: $\hat{s}$ is the dimensional distance along the centreline from a specified origin, O, and $(\hat{r}, \theta)$ are polar coordinates in the plane of cross-section of the tube (figure 1); $(\boldsymbol{e}_r, \boldsymbol{e}_\theta, \boldsymbol{e}_s)$ denote the curvilinear coordinate directions. The tube wall is taken to be at $\hat{r} = a$. We consider a change in coordinate system from the inertial Cartesian coordinate system $(\hat{x}, \hat{y}, \hat{z})$, where the centreline moves in the $(\hat{x}, \hat{y})$-plane, to the non-inertial system $(\hat{r}, \theta, \hat{s})$.

We postulate that one cross-section, at $\hat{s} = 0$, is fixed with its centre at the origin and the tangent to the centreline locally in the $\boldsymbol{e}_y$-direction. The equations are written in terms of the velocity relative to that of the tube wall, so that the no-slip boundary condition for viscous flow at the tube wall can be applied simply; $\hat{\boldsymbol{u}} = (\hat{u}, \hat{v}, \hat{w})$ are the velocity components in the $(\boldsymbol{e}_r, \boldsymbol{e}_\theta, \boldsymbol{e}_s)$ directions and $\hat{R}$ is the radius of curvature. The curvature ratio, δ, is given by $\delta = a/\hat{R}$. (Here 'hats' denote dimensional quantities.) The variables are non-dimensionalized as follows:

$$\left.\begin{aligned} &(\hat{u}, \hat{v}, \hat{w}) \to U_0(u, v, w), \\ &(\hat{r}, \hat{s}) \to a(r, s), \\ &\hat{R} \to aR, \\ &\hat{p} \to \rho U_0^2 p, \\ &\hat{t} \to T t, \end{aligned}\right\} \tag{2.2}$$

where U_0 is a suitable velocity scale and T is the period of the oscillations. The non-dimensional governing equations are then:
continuity

$$u_r + \frac{1}{r}v_\theta + \frac{1}{h}w_s + \frac{1}{r}u + \frac{\delta\,\cos\theta}{h}u - \frac{\delta\,\sin\theta}{h}v + \frac{\alpha^2\,\dot{\delta} r\,\cos\theta}{Re\,h} = 0, \tag{2.3a}$$

$\boldsymbol{e}_r$

$$\frac{\alpha^2}{Re}u_t + uu_r + \frac{1}{r}vu_\theta + \frac{1}{h}wu_s - \frac{1}{r}v^2 + \frac{\alpha^4}{Re^2}\cos\theta\left(-\frac{\ddot{\delta}}{\delta^2} + \frac{2\dot{\delta}^2}{\delta^3}\right)(1-\cos s\delta) - \frac{\alpha^2}{Re}s\dot{\delta}\cos\theta\left(2w + \frac{\alpha^2}{Re}\frac{s\dot{\delta}h}{\delta}\right) - \frac{\delta\ \cos\theta}{h}w^2 = -p_r - \frac{1}{Re\,rh}\left\{\frac{\partial}{\partial\theta}\left[\frac{h}{r}(v + rv_r - u_\theta)\right] - \frac{\partial}{\partial s}\left[\frac{r}{h}(-\delta\ \cos\theta\, w - hw_r + u_s)\right]\right\} - \frac{2\alpha^2\dot{\delta}\ \cos\theta}{Re^2\,h}, \tag{2.3b}$$

$\boldsymbol{e}_\theta$

$$\frac{\alpha^2}{Re}v_t + uv_r + \frac{1}{r}vv_\theta + \frac{1}{h}wv_s + \frac{1}{r}uv - \frac{\alpha^4}{Re^2}\sin\theta\left(-\frac{\ddot{\delta}}{\delta^2} + \frac{2\dot{\delta}^2}{\delta^3}\right)(1-\cos s\delta) + \frac{\alpha^2}{Re}s\dot{\delta}\sin\theta\left(2w + \frac{\alpha^2}{Re}\frac{s\dot{\delta}h}{\delta}\right) + \frac{\delta\ \sin\theta}{h}w^2 = -\frac{1}{r}p_\theta + \frac{1}{Re\,h}\left\{\frac{\partial}{\partial r}\left[\frac{h}{r}(v + rv_r - u_\theta)\right] - \frac{\partial}{\partial s}\left[\frac{1}{rh}(-\delta r\ \sin\theta\, w + hw_\theta - rv_s)\right]\right\} + \frac{2\alpha^2\dot{\delta}\ \sin\theta}{Re^2\,h}, \tag{2.3c}$$

$\boldsymbol{e}_s$

$$\frac{\alpha^2}{Re}w_t + uw_r + \frac{1}{r}vw_\theta + \frac{1}{h}ww_s + \frac{\alpha^4}{Re^2}\left(-\frac{\ddot{\delta}}{\delta^2} + \frac{2\dot{\delta}^2}{\delta^3}\right)\sin s\delta + 2\frac{\alpha^2}{Re}s\dot{\delta}\cos\theta\, u - 2\frac{\alpha^2}{Re}s\dot{\delta}\sin\theta\, v - \frac{2\alpha^4 s\dot{\delta}^2}{Re^2\,\delta^2} + \frac{\alpha^4 s\ddot{\delta}h}{Re^2\,\delta} + \frac{\delta\ \cos\theta}{h}uw - \frac{\delta\ \sin\theta}{h}vw + \frac{\alpha^2\dot{\delta}r\cos\theta}{Re\,h}w = -\frac{1}{h}p_s + \frac{1}{Re\,r}\left\{\frac{\partial}{\partial\theta}\left[\frac{1}{hr}(hw_\theta - \delta r\ \sin\theta\, w - rv_s)\right] - \frac{\partial}{\partial r}\left[\frac{r}{h}(-hw_r - \delta\ \cos\theta\, w + u_s)\right]\right\}. \tag{2.3d}$$

Here

$$h = [1 + \delta(t)\,r\ \cos\theta] \tag{2.4}$$

and is $1/R$ times the distance from the centre of curvature of the centreline (at a particular s) to the projection on the plane containing the centreline of a general point (r, θ, s). The boundary conditions are that

$$\boldsymbol{u} = (u, v, w) = 0 \quad \text{on} \quad r = 1. \tag{2.5}$$

α is the dimensionless frequency, known as Womersley's parameter, and Re is the Reynolds number; they are defined by

$$\alpha = \left(\frac{a^2}{\nu T}\right)^{1/2}, \quad Re = \frac{U_0\,a}{\nu}. \tag{2.6}$$

In the analysis that follows, it is convenient to follow Lyne (1971) and take the velocity scale U_0 equal to ν/a so that formally $Re = 1$. Physically, α^2 is the ratio of the frequency of the oscillations to the inverse time scale for viscous diffusion of momentum across the boundary layer. Thus for small values of α the flow is essentially quasi-steady and is viscous throughout. However, for large values of α the rate of viscous diffusion is small compared with the frequency and the effects of viscous diffusion are confined to thin layers on the boundary.

In equation (2.3*b*) the term $\alpha^4 \cos\theta\,(-\ddot{\delta}/\delta^2 + 2\dot{\delta}^2/\delta^3)\,(1-\cos s\delta)$ is the first new term due to time-dependence of curvature. It results from the acceleration of the frame of reference. The next term, $-\alpha^2 s\dot{\delta}\cos\theta\, 2w$ is a 'Coriolis' force associated with the rotation of the frame of reference. The term $-\alpha^2 s\dot{\delta}\cos\theta\,\alpha^2(s\dot{\delta}h/\delta)$ is a combination of a centrifugal-force-type term resulting from the rotation of the reference frame and a term due to the acceleration of the frame of reference. The final term in equation (2.3*b*) is a viscous term associated with the deformation of the frame of reference. The origin of the new terms is similar for equation (2.3*c*). In equation (2.3*d*), the terms $2\alpha^2 s\dot{\delta}\cos\theta\, u$ and $-2\alpha^2 s\dot{\delta}\sin\theta\, v$ are 'Coriolis' force terms, $(-2\alpha^4 s\dot{\delta}^2/\delta^2$ results from the reference frame acceleration and $(\alpha^4 s\ddot{\delta}h)/\delta$ derives from acceleration terms and a centrifugal force term. The additional 'new' inertia term is the one linear in w at the end of the third line of (2.3*d*); this cannot be attributed to any classical 'forces' seen in the systems translating and rotating with uniform acceleration and angular velocity, and represents spatial variations in these quantities. All the other terms in equations (2.3*b–d*) arise also in flow in a fixed curved pipe (see Pedley 1980, chapter 4).

We shall consider the curvature to be

$$\delta = \delta_0(1 + \epsilon \sin t), \tag{2.7}$$

so that the variation of curvature with time is assumed to be sinusoidal. Here δ_0 is the mean curvature and ϵ represents the amplitude of its oscillations. We shall take both δ_0 and ϵ to be small, so that the curvature is small and varies only by a small amount. Note that $\dot{\delta} = \delta_0 \epsilon \cos t$ and $\ddot{\delta} = -\delta_0 \epsilon \sin t$. Now $\delta = 1/R$ and so $\dot{\delta} = -\dot{R}/R^2$. Thus $\cos t > 0$ corresponds to $\dot{R} < 0$, i.e. to the radius of curvature decreasing with time (negative rotation). Similarly, $\cos t < 0$ corresponds to the radius of curvature increasing with time (positive rotation). The dimensionless axial pressure gradient is given by

$$-p_s = \alpha^2 W_p \cos(t + \Phi), \tag{2.8}$$

where W_p is the dimensionless velocity amplitude that would be driven by such a pressure gradient in a straight pipe containing an inviscid fluid and Φ represents the phase difference between the oscillatory pressure gradient and the time-dependent curvature. Note that because the chosen velocity scale is ν/a, W_p is a Reynolds number for the primary axial flow.

One important feature of curved tube flow is the secondary motion that arises in the cross-sectional plane. This secondary motion itself influences the distribution of axial velocity and results in a complicated interaction of the two. We shall determine the secondary flows that arise due to both the mean and the time-dependent curvature components. We are particularly interested in the non-zero mean part of the secondary flow and its influence on the axial flow and in the magnitude and distribution of the resulting wall shear stress perturbations. The axial and azimuthal components of

dimensionless wall shear stress are defined as follows:

$$\text{Axial wall shear stress} \;=\; -w_r|_{r=1}, \tag{2.9a}$$

$$\text{Azimuthal wall shear stress} \;=\; -v_r|_{r=1}. \tag{2.9b}$$

2.2. *Derivation of the secondary streaming Reynolds numbers when* $\alpha \gg 1$

The secondary flow behaviour, in the cross-sectional plane of the tube, is determined by the secondary streaming Reynolds numbers, R_s and R_{s_1}. These are derived in the same way as a conventional Reynolds number except that the velocity scales used are the characteristic secondary velocity scales. The secondary velocity that arises due to the mean curvature of the tube leads to one velocity scale, while the secondary velocity generated by the time-dependence of curvature leads to another. These scales may be found by inspection of equations (2.3*a–d*) and are the same for both the low and high frequency cases. However, the interpretation of the secondary streaming Reynolds numbers as the controlling parameters for the secondary flow behaviour is most clearly seen by considering the large-α case, as detailed below. The quantities obtained are equally applicable to the small-α case.

Lyne (1971) examined flow driven by a high-frequency pressure gradient in a fixed, weakly curved pipe. Here we extend Lyne's analysis to the case of a tube with time-dependent curvature. As in the fixed curved tube case, at large values of α, we expect the flow to consist of an inviscid core surrounded by a viscous Stokes boundary layer, of dimensionless thickness $O(1/\alpha)$, on the boundary at $r = 1$. In the core of the pipe, a balance exists between the centrifugal forces that arise due to the curvature of the pipe, the new terms introduced by the time-dependent curvature and the pressure gradient in that plane. In the Stokes layer the value of w, the axial velocity, must be zero at the wall (no-slip condition). Thus in the boundary layer there will no longer be a balance between the pressure gradient and the centrifugal and Coriolis force terms since the pressure gradient remains essentially unchanged while the latter terms, which are proportional to w, have diminished. Thus oscillatory secondary motions, primarily consisting of a θ-component of velocity, v, are generated by the interaction of the local inertia term and the viscous forces with the centrifugal and Coriolis forces respectively. The solution for v will contain an oscillation of double the fundamental frequency, and a mean flow. These secondary flows must satisfy the no-slip condition at the boundary. However, it is impossible also to impose the condition that these flows tend to zero at the edge of the Stokes layer. Instead, the secondary motions 'drag' the fluid in the core of the tube, thus generating secondary motions there. The details of the core flow will depend on the value of the secondary streaming Reynolds numbers, R_s and R_{s_1} (see below).

We take the curvature to be small and thus consider a small-parameter expansion in powers of δ_0:

$$\left.\begin{aligned} u &= u_0 + (2\delta_0)u_1 + \cdots, \\ v &= v_0 + (2\delta_0)v_1 + \cdots, \\ w &= w_0 + (2\delta_0)w_1 + \cdots, \\ p &= p_0 + (2\delta_0)p_1 + \cdots. \end{aligned}\right\} \tag{2.10}$$

If the viscous terms in equations (2.3*a*)–(2.3*d*) are dropped, they have a solution,

satisfying $u = 0$ at $r = 1$, in which the velocity and pressure distributions are

$$\left.\begin{aligned} u &= (2\delta_0)\left[-\tfrac{3}{16}\alpha^2\epsilon\,\cos\theta\,(1-r^2)\,\cos t\right] + O((2\delta_0)^2),\\ v &= (2\delta_0)\left[\tfrac{3}{16}\alpha^2\epsilon\,\sin\theta\,(1-\tfrac{1}{3}r^2)\,\cos t\right] + O((2\delta_0)^2),\\ w &= W_p\sin(t+\Phi) + (2\delta_0)\left[-\alpha^4\,\epsilon r\cos\theta\, s\cos t + O(\alpha^2)\times\text{s-indep. terms}\right] + O((2\delta_0)^2),\\ p &= (2\delta_0)\left[\alpha^2\epsilon W_p\, r\,\cos\theta\, s\,\cos t\sin(t+\Phi) - \alpha^2\epsilon r\,\cos\theta\,\cos t\right.\\ &\quad -\tfrac{1}{4}\alpha^4\epsilon r\,\cos\theta\, s^2\,\sin t + \tfrac{1}{2}(1+\epsilon\sin t)\,W_p^2 r\,\cos\theta\,\sin^2(t+\Phi)\\ &\quad \left.-\tfrac{3}{16}\alpha^4\,\epsilon\,(r-\tfrac{1}{3}r^3)\,\cos\theta\,\sin t\right] + O((2\delta_0)^2). \end{aligned}\right\} \tag{2.11}$$

This can be considered as the primary core flow. In a fixed curved pipe there is no secondary flow in the plane of cross-section as there is a balance between the centrifugal force terms and the pressure gradient in that plane. Here the introduction of time-dependent curvature results in non-zero radial and azimuthal velocities, u and v. These are necessary in order that the continuity equation, (2.3a), is satisfied at $O(2\delta_0)$. The fluid pressure adjusts in order to balance the s-dependent Coriolis forces that arise due to the rotation of the frame of reference, the s^2-dependent terms that arise due to the translation of the frame of reference and the viscous terms associated with the deformation of the frame of reference (see equations (2.3b, c)). There is also an adjustment to balance the local inertial terms in (2.3b, c), involving the new radial and circumferential velocities. Note that the secondary velocities and the pressure distribution are $O(2\delta_0)$ compared with the leading-order axial velocity, and thus are much smaller.

We are interested in determining the magnitude of the secondary velocities that are generated in the boundary layer, since from these the secondary streaming Reynolds numbers can be derived.

For $\alpha \gg 1$, we introduce the boundary-layer coordinate

$$\eta = \frac{\alpha}{\sqrt{2}}(1-r). \tag{2.12}$$

Solutions are sought of the form:

$$\left.\begin{aligned} w &= W_0 + (2\delta_0)W_1 + (2\delta_0)^2 W_2 + \cdots,\\ u &= U_0 + (2\delta_0)U_1 + (2\delta_0)^2 U_2 + \cdots,\\ v &= V_0 + (2\delta_0)V_1 + (2\delta_0)^2 V_2 + \cdots,\\ p &= P_0 + (2\delta_0)P_1 + (2\delta_0)^2 P_2 + \cdots; \end{aligned}\right\} \tag{2.13}$$

u, v and w must satisfy the no-slip boundary condition at $\eta = 0$, and must match the core flow as $\eta \to \infty$.

Substitution of (2.12) and (2.13) into the governing equations (2.3a–d) gives the boundary layer equations at successive orders of $(2\delta_0)$.

The equations at $O((2\delta_0)^0)$ are just the boundary layer equations for flow in a straight tube driven by an oscillatory axial pressure gradient. The solution to these equations that matches with the core and satisfies the no-slip condition at the boundary is the Stokes layer flow:

$$U_0 = 0, \quad V_0 = 0, \quad W_0 = W_p\left(\sin(t+\Phi) - \mathrm{e}^{-\eta}\sin(t+\Phi-\eta)\right), \quad P_0 = 0. \tag{2.14}$$

Thus at leading order there are no components of secondary velocity and the axial

velocity adjusts to satisfy the no-slip condition. New terms are introduced into the governing equations by the time-dependence of curvature only at $O(2\delta_0)$:
continuity

$$-(\alpha/\sqrt{2})U_{1\eta} + \frac{1}{(1-(\sqrt{2}/\alpha)\eta)}V_{1\theta} + \frac{1}{(1-(\sqrt{2}/\alpha)\eta)}U_1 + W_{1s}$$
$$+\tfrac{1}{2}(1+\epsilon\,\sin t)\,\cos\theta\,U_0 - \tfrac{1}{2}(1+\epsilon\,\sin t)\,\sin\theta V_0$$
$$+\tfrac{1}{2}\alpha^2\epsilon\,(1-(\sqrt{2}/\alpha)\eta)\cos\theta\,\cos t = 0, \tag{2.15a}$$

$\boldsymbol{e}_r$

$$\alpha^2 U_{1t} - (\alpha/\sqrt{2})(U_0U_{1\eta} + U_1U_{0\eta}) + \frac{1}{(1-(\sqrt{2}/\alpha)\eta)}(V_0U_{1\theta} + V_1U_{0\theta})$$
$$+W_0U_{1s} + W_1U_{0s} - \tfrac{1}{2}(1+\epsilon\,\sin t)\,(1-(\sqrt{2}/\alpha)\eta)\,\cos\theta W_0U_{0s}$$
$$-\frac{2}{(1-(\sqrt{2}/\alpha)\eta)}V_0V_1 + \tfrac{1}{4}\alpha^4\epsilon\,\cos\theta\,s^2\,\sin t - \alpha^2\epsilon\,\cos\theta\,s\cos t W_0$$
$$-\tfrac{1}{2}(1+\epsilon\,\sin t)\,\cos\theta W_0^2 = (\alpha/\sqrt{2})\frac{\partial P_1}{\partial\eta} - \frac{1}{(1-(\sqrt{2}/\alpha)\eta)}$$
$$\times\left\{\frac{\partial}{\partial\theta}\left[\frac{1}{(1-(\sqrt{2}/\alpha)\eta)}\times(V_1-(\alpha/\sqrt{2})(1-(\sqrt{2}/\alpha)\eta)V_{1\eta}-U_{1\theta})\right]\right.$$
$$\left.-\frac{\partial}{\partial s}[(1-(\sqrt{2}/\alpha)\eta)((\alpha/\sqrt{2})W_{1\eta}+U_{1s})]\right\} - \alpha^2\epsilon\,\cos\theta\,\cos t, \tag{2.15b}$$

and similarly for $\boldsymbol{e}_\theta$,
$\boldsymbol{e}_s$

$$\alpha^2 W_{1t} - (\alpha/\sqrt{2})(U_0W_{1\eta} + U_1W_{0\eta}) + \frac{1}{(1-(\sqrt{2}/\alpha)\eta)}(V_0W_{1\theta} + V_1W_{0\theta})$$
$$+W_0W_{1s} + W_1W_{0s} + \alpha^2\epsilon\,\cos\theta\,s\,\cos tU_0 - \alpha^2\epsilon\,\sin\theta\,s\,\cos tV_0$$
$$-\tfrac{1}{2}\,\alpha^4\epsilon\,(1-(\sqrt{2}/\alpha)\eta)\,\cos\theta\,s\,\sin t$$
$$= -P_{1s} + \tfrac{1}{2}(1+\epsilon\,\sin t)\,\cos\theta\,(1-(\sqrt{2}/\alpha)\eta)\,P_{0s}$$
$$+\frac{1}{(1-(\sqrt{2}/\alpha)\eta)}\left\{\frac{\partial}{\partial\theta}\left(\frac{1}{(1-(\sqrt{2}/\alpha)\eta)}W_{1\theta}\right)+(\alpha/\sqrt{2})\frac{\partial}{\partial\eta}((\alpha/\sqrt{2})W_{0\eta})\right\}. \tag{2.15c}$$

An expansion in powers of $(1/\alpha)$ is proposed:

$$\left.\begin{aligned} W_1 &= \alpha^2(W_{10} + (1/\alpha)W_{11} + \cdots),\\ U_1 &= \alpha^2(U_{10} + (1/\alpha)U_{11} + \cdots),\\ V_1 &= \alpha^2(V_{10} + (1/\alpha)V_{11} + \cdots),\\ P_1 &= \alpha^4(P_{10} + (1/\alpha)P_{11} + \cdots). \end{aligned}\right\} \tag{2.16}$$

(Here we have assumed that α is large, but still $\delta_0 \ll 1/\alpha^2 \ll 1$.)

At leading order equation (2.15*a*) gives

$$-\frac{1}{\sqrt{2}}U_{10\eta} = 0 \tag{2.17}$$

which, together with the boundary condition that $U_{10} = 0$ on $\eta = 0$, implies that $U_{10} \equiv 0$.

Equation (2.15*b*) gives that $P_{10\eta} = 0$ and so, matching with the pressure in the core given by (2.11), we have

$$P_{10} = -\tfrac{1}{8}\epsilon\, \cos\theta\, \sin t - \tfrac{1}{4}\epsilon\, \cos\theta\, s^2 \sin t. \tag{2.18}$$

The leading-order $\mathbf{e}_\theta$ equation simplifies to

$$V_{10t} - \tfrac{1}{2}V_{10\eta\eta} = -\tfrac{1}{8}\epsilon\, \sin\theta\, \sin t. \tag{2.19}$$

The solution for V_{10}, that satisfies no-slip and the matching condition given by (2.11), is

$$V_{10} = \tfrac{1}{8}\epsilon\, \sin\theta\, \left[\cos t - \mathrm{e}^{-\eta}\, \cos(t-\eta)\right]. \tag{2.20}$$

By considering the axial equation at leading order we find that

$$W_{10} = -\epsilon\, \cos\theta\, s\, \left[\cos t - \mathrm{e}^{-\eta} \cos(t-\eta)\right]; \tag{2.21}$$

these both represent Stokes layers driven by the $O(2\delta_0)$ primary core flow.

Similarly, the $\boldsymbol{e}_r$ and $\boldsymbol{e}_\theta$ equations, at $O(\alpha^4)$ and $O(\alpha^3)$ respectively, give that

$$P_{11} = \tfrac{1}{4}\sqrt{2}\epsilon\eta\, \cos\theta\, s^2\, \sin t, \tag{2.22}$$

and

$$V_{11} = -\tfrac{1}{8}\sqrt{2}\epsilon\eta\, \sin\theta\, \cos t - \tfrac{1}{16}\sqrt{2}\eta\, \mathrm{e}^{-\eta}\epsilon \sin\theta \cos(t-\eta). \tag{2.23}$$

V_{11}, like V_{10}, is driven by the primary core flow. The continuity equation, (2.15*a*), at $O(\alpha^2)$ gives

$$U_{11} = -\tfrac{3}{8}\sqrt{2}\epsilon\eta \cos\theta \cos t + \tfrac{7}{8}\epsilon \cos\theta\, \left[\sin(t-\eta+\tfrac{1}{4}\pi) - \mathrm{e}^{-\eta} \sin(t-\eta+\tfrac{1}{4}\pi)\right]. \tag{2.24}$$

Note that U_{11} does not match the core velocity as $\eta \to \infty$ (a displacement effect, present in all boundary layers).

Equation (2.15*b*) at $O(\alpha^3)$ gives

$$\frac{1}{\sqrt{2}}P_{12\eta} = \tfrac{3}{8}\sqrt{2}\epsilon\eta \cos\theta \sin t - \tfrac{7}{16}\sqrt{2}\epsilon \cos\theta \sin t + \tfrac{7}{16}\sqrt{2}\epsilon \cos\theta \cos t, \tag{2.25}$$

and so

$$P_{12} = \tfrac{3}{8}\epsilon\eta^2 \cos\theta \sin t + \tfrac{7}{8}\epsilon\eta \cos\theta\, (\cos t - \sin t) - \epsilon \cos\theta \cos t + \epsilon W_p \cos\theta\, s\, \sin(t+\Phi)\cos t. \tag{2.26}$$

The $\boldsymbol{e}_\theta$ equation at $O(\alpha^2)$ is

$$V_{12t} - \tfrac{1}{2}V_{12\eta\eta} + \epsilon \sin\theta\, s\, \cos t W_0 = -P_{12\theta} - \sqrt{2}\eta P_{11\theta} - 2\eta^2 P_{10\theta} + \text{viscous terms}. \tag{2.27}$$

The terms on the right-hand side of (2.27) will lead to a contribution to V_{12} that is driven by the primary core flow. However, the term $\epsilon \sin\theta s \cos t W_0$ will lead to a contribution to V_{12} that is $O(\epsilon W_p)$. This contribution to V_{12} is the first Stokes layer secondary velocity that is not driven by the primary core flow. It is generated by the Coriolis terms that arise because the pipe under consideration has time-dependent curvature.

P_{13} is determined from the radial equation (2.15*b*) at $O(\alpha^2)$ and at $O(\alpha)$ the equation for V_{13}, obtained from the $\mathbf{e}_\theta$ equation is

$$V_{13t} - \tfrac{1}{2}V_{13\eta\eta} + \epsilon \sin\theta\, s \cos t W_{01} = -P_{13\theta} - \sqrt{2}\eta P_{12\theta} - 2\eta^2 P_{11\theta} - 2\sqrt{2}\eta^3 P_{10\theta} + \text{viscous terms.} \quad (2.28)$$

Again, the terms on the right-hand side of equation (2.28) will lead to a contribution to V_{13} that is driven by the primary core flow. Moreover, since $W_{01} = 0$, the term on the left-hand side of the equation does not yield any secondary velocities.

Equation (2.15*b*) at $O(\alpha)$ gives P_{14} and the $\boldsymbol{e}_\theta$ equation at $O(1)$ gives

$$V_{14t} - \tfrac{1}{2}V_{14\eta\eta} + \frac{(1+\epsilon\sin t)\sin\theta}{2} W_0^2 = -P_{14\theta} - \sqrt{2}\eta P_{13\theta} - 2\eta^2 P_{12\theta} - 2\sqrt{2}\eta^3 P_{11\theta} - 4\eta^4 P_{10\theta} + \text{viscous terms.} \quad (2.29)$$

As before, the terms on the right-hand side lead to a primary core flow driven component of V_{14}. However the term $(1+\epsilon\sin t)\sin\theta W_0^2/2$ will generate a contribution to V_{14}, which will have a non-zero mean since the product W_0^2 contains time-independent terms. It is easily seen that, since $W_0 = O(W_p)$, $V_{14} = O(W_p^2)$. This is the scale of the secondary velocity that is generated in the Stokes layer by the centrifugal force effects that arise because the tube is curved. (V_{14} is just Lyne's quasi-steady secondary velocity.)

The solutions of (2.27) and (2.29) do not match to the core solutions as $\eta \to \infty$. The solutions for both V_{12} and V_{14} satisfy the no-slip condition at the boundary, but, in both cases, the velocity does not fall to zero as $\eta \to \infty$. Instead, these secondary motions 'drag' the fluid in the core of the tube, thus generating secondary motions outside the boundary layer. For non-zero Φ, both V_{12} and V_{14} will generate steady secondary streaming in the core.

Putting these results back into dimensional form, we obtain

$$\hat{V}_{12\infty} = O(v\epsilon W_p(2\delta_0)/a) \quad (2.30)$$

and

$$\hat{V}_{14\infty} = O(v W_p^2(2\delta_0)/(a\alpha^2)) \quad (2.31)$$

where $\hat{V}_{12\infty}$ and $\hat{V}_{14\infty}$ are the velocities at the edge of the Stokes layer.
Thus the secondary streaming Reynolds numbers are defined to be

$$\left.\begin{aligned} R_{s_1} &= \hat{V}_{12\infty}\, a/v = \epsilon W_p(2\delta_0), \\ 2R_s &= \hat{V}_{14\infty}\, a/v = W_p^2(2\delta_0)/\alpha^2. \end{aligned}\right\} \quad (2.32)$$

R_s is the secondary streaming Reynolds number based on the scale of the secondary velocity that arises because the tube is curved, and is the same as that determined by Lyne for a fixed curved tube. R_{s_1} is the secondary streaming Reynolds number based on the scale of the secondary velocity that arises from the time-dependence of curvature.

Substitution of δ, $\dot{\delta}$ and $\ddot{\delta}$ into equations (2.3*a–d*) reveals that the product of $\alpha\epsilon$ frequently occurs. Thus we define a new parameter, R_t, as

$$R_t = \alpha\epsilon = R_{s_1}/[(2R_s)^{1/2}(2\delta_0)^{1/2}]. \quad (2.33)$$

2.3. *Parameter scalings*

Equations (2.3*a–d*) are very complicated and cannot be solved as they stand. In order to simplify the problem and to isolate the effects of the various new terms upon the magnitude and distribution of wall shear stress, and the generation of steady secondary streaming, various perturbative techniques are carried out.

The four governing parameters of the problem are δ_0, R_t, $(2R_s)^{1/2}$ and α. In this paper we examine one particular choice of parameter scalings. Initially α and R_s are chosen to be order one compared with δ_0 and R_t, although they are later taken to be either large or small. We shall consider δ_0 to be the smallest parameter of the problem and take $\delta_0 \to 0$, while keeping $R_t = O(1)$. R_t is then taken to be small because $\epsilon \ll 1$. (ϵ is chosen to be sufficiently small that R_t can be taken to be small even in the case where $\alpha \gg 1$, as in § 5.) We shall show that the leading-order flow is just that driven by an oscillatory pressure gradient in a fixed curved pipe (§ 3). At $O(R_t)$, effects due to the unsteadiness of the curvature are first seen. The details of this problem are described in §§ 4, 5 for low and high frequencies respectively.

3. Perturbation to oscillatory flow in a fixed, curved pipe

We now proceed to solve equations (2.3*a–d*) together with the boundary condition (2.5) for flows driven by both low- and high-frequency pressure gradients subject to the parameter scaling discussed in § 2.3.

The axial velocity is rescaled so that the centrifugal force terms in the governing equations are formally the same order of magnitude as the viscous and inertial terms. Thus we take $w \to \overline{w}/(2\delta_0)^{1/2}$; we also take $s \to \bar{s}/(2\delta_0)^{1/2}$. δ, $\dot{\delta}$ and $\ddot{\delta}$ are substituted into (2.3*a–d*) and R_t is defined as in (2.33). Note that $-\partial p(\bar{s})/\partial \bar{s} = \alpha^3(2R_s)^{1/2}\cos(t+\Phi)/(2\delta_0)^{1/2}$. Since δ_0 is the smallest parameter of the problem, we delete all terms that are $O(\delta_0)$ relative to the leading terms. Next a small-parameter expansion is carried out in powers of R_t:

$$\left.\begin{aligned} \overline{w} &= \overline{w}_0 + R_t\,\overline{w}_1 + \cdots, \\ \overline{u} &= \overline{u}_0 + R_t\,\overline{u}_1 + \cdots, \\ \overline{v} &= \overline{v}_0 + R_t\,\overline{v}_1 + \cdots, \\ \overline{p} &= \overline{p}_0 + R_t\,\overline{p}_1 + \cdots, \end{aligned}\right\} \tag{3.1}$$

and we consider the equations at various orders of R_t. At leading order, $O(R_t^0)$, the equations are the same as for flow in a fixed curved pipe.

At $O(R_t)$ the equations are (dropping overbars):

continuity:

$$u_{1r} + \frac{1}{r}v_{1\theta} + w_{1s} + \frac{1}{r}u_1 = 0, \tag{3.2a}$$

$\boldsymbol{e}_r$:

$$\begin{aligned} &\alpha^2 u_{1t} + u_0\,u_{1r} + u_1 u_{0r} + \frac{1}{r}v_0\,u_{1\theta} + \frac{1}{r}v_1 u_{0\theta} + w_0\,u_{1s} + w_1 u_{0s} - \frac{2}{r}v_0\,v_1 \\ &\quad + \tfrac{1}{4}\alpha^3\cos\theta\,s^2\sin t - \alpha\cos\theta\,s\cos t\,w_0 - \cos\theta\,w_0 w_1 - \frac{1}{\alpha}\cos\theta\sin t\,w_0^2 \\ &\quad = -p_{1r} - \frac{1}{r}\left\{\frac{\partial}{\partial\theta}\left[\frac{1}{r}(v_1 + rv_{1r} - u_{1\theta})\right] - \frac{\partial}{\partial s}(-rw_{1r})\right\}, \end{aligned} \tag{3.2b}$$

$\boldsymbol{e}_\theta$:

$$\alpha^2 v_{1t} + u_0 v_{1r} + u_1 v_{0r} + \frac{1}{r} v_0 v_{1\theta} + \frac{1}{r} v_1 v_{0\theta} + w_0 v_{1s} + w_1 v_{0s} + \frac{1}{r}(u_0 v_1 + u_1 v_0)$$
$$- \tfrac{1}{4}\alpha^3 \sin\theta\, s^2 \sin t + \alpha \sin\theta\, s \cos t\, w_0 + \sin\theta\, w_0 w_1 + \frac{1}{\alpha} \sin\theta \sin t\, w_0^2$$
$$= -\frac{1}{r} p_{1\theta} + \left\{ \frac{\partial}{\partial r}\left[\frac{1}{r}(v_1 + r v_{1r} - u_{1\theta})\right] - \frac{\partial}{\partial s}\left(\frac{1}{r} w_{1\theta}\right)\right\}, \tag{3.2c}$$

$\boldsymbol{e}_s$:

$$\alpha^2 w_{1t} + u_0 w_{1r} + u_1 w_{0r} + \frac{1}{r}(v_0 w_{1\theta} + v_1 w_{0\theta}) + w_0 w_{1s} + w_1 w_{0s} = \nabla^2 w_1. \tag{3.2d}$$

Thus at this order, effects due to the time-dependence of curvature are present. Note that new terms exist in equations (3.2*b*, *c*) but there are no additional new terms to the axial momentum equation (3.2*d*). By assuming $R_t \ll 1$ we have taken $R_{s_1} \ll (2R_s)^{1/2}$ (see equation (2.33)) so that the velocity at the edge of the Stokes layer that arises due to the time-dependence of curvature is less than that arising because the tube is curved.

4. Low frequency

4.1. *Solution*

In this section we consider flows at low frequency, $\alpha \ll 1$ (in fact $\delta_0 \ll R_t \ll \alpha \ll 1$). We therefore consider a small-parameter expansion in powers of α. R_s is assumed to remain $O(1)$ compared with the other governing parameters.

At $O(R_t^0)$, the equations for flow in a fixed curved pipe are obtained (Mullin & Greated 1980*b*). The radial and azimuthal equations may be combined in a single equation for the streamfunction, ψ_0. The following expansions for the axial velocity, w_0, and the streamfunction, ψ_0, are then considered:

$$\left.\begin{aligned} w_0 &= \alpha^3 w_{00} + \alpha^4 w_{01} + \cdots, \\ \psi_0 &= \alpha^6 \psi_{00} + \alpha^7 \psi_{01} + \cdots. \end{aligned}\right\} \tag{4.1}$$

The leading-order axial velocity, driven by the applied oscillatory pressure gradient, is just

$$w_{00} = \tfrac{1}{4}(2R_s)^{1/2}(1 - r^2)\cos(t + \Phi). \tag{4.2}$$

Thus the leading-order axial wall shear stress is

$$-w_{00r}|_{r=1} = \tfrac{1}{2}(2R_s)^{1/2} \cos(t + \Phi). \tag{4.3}$$

The balance of the local inertia term with the viscous term in the axial velocity equation leads to the following further corrections to the axial velocity:

$$\left.\begin{aligned} w_{01} &= 0, \\ w_{02} &= \tfrac{1}{64}(2R_s)^{1/2}(3 - r^2)(1 - r^2) \sin(t + \Phi), \\ w_{03} &= 0, \\ w_{04}^a &= \tfrac{1}{64}(2R_s)^{1/2}(-\tfrac{19}{36} + \tfrac{3}{4}r^2 - \tfrac{1}{4}r^4 + \tfrac{1}{36}r^6)\cos(t + \Phi). \end{aligned}\right\} \tag{4.4}$$

Both w_{02} and w_{04}^a are symmetric in r. Note that we let $w_{04} = w_{04}^a + w_{04}^b$ since the axial velocity at this order consists of two parts: a symmetric part, w_{04}^a, and a term, w_{04}^b,

that is asymmetric in r (see below). The leading-order streamfunction is

$$\psi_{00} = \frac{1}{8 \times 144} R_s\, r(1-r^2)^2\,(1-\tfrac{1}{4}r^2)\sin\theta\cos^2(t+\Phi). \tag{4.5}$$

The leading-order azimuthal wall shear stress, (2.9b), is

$$\psi_{00rr}|_{r=1} = \tfrac{1}{192}\, R_s\, \sin\theta\cos^2(t+\Phi). \tag{4.6}$$

Equations (4.2) and (4.5) are the quasi-steady equivalent of the leading-order Poiseuille axial velocity and streamfunction found for Dean flow. The term $(1/r)\,\psi_{00\theta}$, proportional to the radial velocity, is positive on $\theta = 0$ (and negative on $\theta = \pi$). Thus, for small frequencies, the steady component of streaming in the core proceeds across the tube from the inside of the bend to the outside (as in Dean flow). This secondary streamfunction advects the leading-order quasi-steady Poiseuille velocity, w_{00}, which results in a 'skewing' of the previously symmetric axial velocity profile. This axial velocity perturbation is

$$w_{04}^b = \frac{1}{45 \times 8^5}(2R_s)^{3/2}\, r(1-r^2)\,(19-21r^2+9r^4-r^6)\,\cos\theta\,\cos^3(t+\Phi). \tag{4.7}$$

Thus the curvature of the pipe leads to the distortion of the axial velocity profile and an increase in the wall shear stress on the outside of the wall. The results are s-independent. At this order there are no new effects due to the unsteadiness of the curvature. In order to understand the effects of time-dependent curvature on the flow, we must consider the equations at $O(R_t)$.

To solve the $O(R_t)$ equations, (3.2a–d), we consider the following small-parameter expansion in powers of α:

$$\left.\begin{aligned} w_1 &= \alpha^7 w_{10} + \alpha^8 w_{11} + \cdots, \\ u_1 &= \alpha^4 u_{10} + \alpha^5 u_{11} + \cdots, \\ v_1 &= \alpha^4 v_{10} + \alpha^5 v_{11}\cdots, \\ p_1 &= \alpha^3 p_{10} + \alpha^4 p_{11} + \cdots. \end{aligned}\right\} \tag{4.8}$$

(The expansion in powers of α is taken to a sufficiently high degree to obtain the first new effects from the time-dependent curvature.)

At $O(\alpha^3)$ equations (3.2b, c) give

$$p_{10} = -\tfrac{1}{4}\, r\,\cos\theta\, s^2\,\sin t; \tag{4.9}$$

the fluid pressure adjusts to balance the new centrifugal-force term that arises from the time-dependence of pipe curvature. It prevents the fluid being 'flung' out along the pipe.

At $O(\alpha^4)$ and $O(\alpha^5)$ equation (3.2a) admits the existence of streamfunctions ψ_{10} and ψ_{11} such that $u_{10} = (1/r)\psi_{10\theta}\,, v_{10} = -\psi_{10r}$ and similarly for u_{11} and v_{11}.

At $O(\alpha^4)$ equations (3.2b, c) can be combined to give

$$\nabla^4\psi_{10} = \tfrac{1}{2}(2R_s)^{1/2} r\,\sin\theta\, s\cos\,t\,\cos(t+\Phi), \tag{4.10}$$

which has solution

$$\psi_{10} = \frac{1}{2 \times 384}(2R_s)^{1/2} r\,(1-r^2)^2\,\sin\theta\, s\,(\cos(2t+\Phi)+\cos\Phi). \tag{4.11}$$

This secondary streaming results from the interaction between the viscous terms and the Coriolis force term that arises from the time-dependence of curvature.

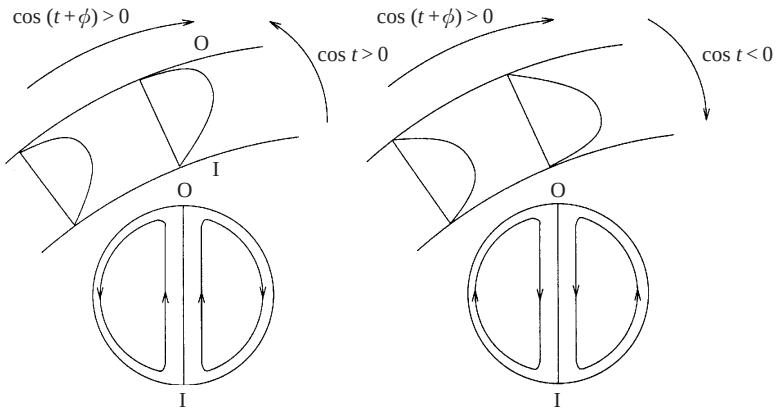

FIGURE 2. Sketch of axial velocity perturbation, w_{10}, with corresponding direction of secondary streaming, ψ_{10}, shown below. For $\cos t > 0$ (negative rotation) and $\cos(t+\Phi) > 0$ (flow in a positive sense) axial velocity skewed towards the outside wall, resulting in increased wall shear stress there. For $\cos t < 0$ and $\cos(t+\Phi) > 0$ the opposite is true.

At leading order (3.2*d*) gives an equation for w_{10} which has solution

$$w_{10} = \tfrac{1}{18432}(2R_s)\cos\theta\, s\cos t\, \cos^2(t+\Phi)\, r(1-r^2)(3-3r^2+r^4). \tag{4.12}$$

4.2. *Discussion*

The first new contribution to the axial velocity from the time-dependence of curvature is w_{10}. It is an $O(R_t)$ perturbation to the axial velocity profile obtained for a fixed curved pipe, and is due to the advection of the leading-order quasi-steady Poiseuille velocity by the new secondary streaming which results in a 'skewing' of the axial velocity profile. This skewing may enhance or diminish the skewing of the axial velocity profile that arises merely due to the pipe being curved.

At any given time t, the direction of the secondary streaming and hence the 'skewing' of the axial velocity depends on the relative signs of $\cos t$ and $\cos(t+\Phi)$ (since $r(1-r^2)^2$ and $r(1-r^2)(3-3r^2+r^4)$ are always positive for r between 0 and 1). For example, if $\cos(t+\Phi)$ is positive, so that the flow is in a positive sense along the pipe, and $\cos t > 0$, so that the pipe is rotating in a negative sense, the streaming is from the inside of the bend to the outside. Thus the skewing of the axial velocity will be towards the outside wall of the pipe, enhancing the effect of pipe curvature and increasing the wall shear stress there. If, however, $\cos t < 0$ while $\cos(t+\Phi) > 0$, the streaming is in the opposite sense and the skewing of the axial velocity profile will be towards the inside wall, increasing the wall shear stress there. The dependence of ψ_{10} on the axial coordinate s means that its influence on the axial velocity profile will become more pronounced as we move away from the fixed origin (figure 2). The new streaming, ψ_{10}, is an order of magnitude smaller than the streaming that results solely from the tube curvature and thus its influence on the axial velocity profile will be small.

We are particularly interested in the properties of the steady components of the secondary streaming and the wall shear stress. The direction of the steady component of the s-dependent secondary streaming, ψ_{10}, depends on the sign of $\cos\Phi$. If $\cos\Phi$ is positive then the steady part of $(1/r)\,\psi_{10\theta}$ is positive on $\theta = 0$ (and negative on $\theta = \pi$) and thus the steady component of the secondary streaming proceeds across the centre

of the pipe from the inside of the bend to the outside, in the same sense as for steady curvature. However, if $\cos\Phi$ is negative then the steady secondary streaming is in the opposite sense. When $\cos\Phi = 0$, i.e. when the time-dependent curvature variations are out of phase with the oscillatory pressure gradient by $\pi/2$, there is no contribution to the steady secondary streaming at this order.

The axial wall shear stress perturbation, due to the advection of w_{00} by the secondary streaming, ψ_{10}, is

$$-w_{10r}|_{r=1} = \tfrac{1}{9216}(2R_s)\cos\theta\, s\cos t\cos^2(t+\Phi), \tag{4.13}$$

and thus, when $\cos t > 0$, the wall shear stress is increased on the outside wall and decreased on the inside wall (with the opposite being the case when $\cos t < 0$.) The azimuthal wall shear stress perturbation, from (4.11), is

$$\psi_{10rr}|_{r=1} = \tfrac{1}{96}(2R_s)^{1/2}\sin\theta\, s(\cos(2t+\Phi)+\cos\Phi). \tag{4.14}$$

In the above analysis R_s is assumed to remain $O(1)$ as all the other parameters tend to zero.

The time-dependency of the secondary streaming, ψ_{10}, means that w_{10} may be very small for certain ranges of t. Within this range, the axial velocity terms at higher powers of α may have an appreciable effect.

5. High frequency

5.1. *Secondary core flow equations*

In this section, the small-R_t perturbation to Lyne's solution for flow driven by a high-frequency oscillatory pressure gradient in a fixed curved pipe is found. We assume that $\delta_0 \ll R_t \ll 1/\alpha^2 \ll 1$ and R_s remains $O(1)$ initially.

At $O(R_t^0)$ the equations are the s-independent equations for flow in a fixed, curved pipe. Lyne (1971) analysed this problem and showed that the leading-order steady streaming in the core $\psi_{00}^{(s)} = R_s\chi_{00}$ is given by the solution to

$$\left.\begin{aligned} &\frac{1}{R_s}\nabla^4\chi_{00} + \frac{1}{r}\left(\chi_{00r}\frac{\partial}{\partial\theta} - \chi_{00\theta}\frac{\partial}{\partial r}\right)\nabla^2\chi_{00} = 0, \\ &\chi_{00} = 0, \quad \chi_{00r} = \tfrac{1}{4}\sin\theta \text{ on } r = 1, \end{aligned}\right\} \tag{5.1}$$

which makes it clear that R_s is the steady streaming Reynolds number (see § 2.2).

As found in § 4 for small α, at leading order the equations contain no new terms due to the unsteadiness of curvature. Thus it is necessary to consider the equations at $O(R_t)$, (3.2*a–d*), which suggest that u_1, v_1, w_1 and p_1 depend on s as follows:

$$\left.\begin{aligned} u_1 &= su_{10} + u_{11}, \\ v_1 &= sv_{10} + v_{11}, \\ w_1 &= w_{10}, \\ p_1 &= s^2p_{10} + sp_{11} + p_{12}. \end{aligned}\right\} \tag{5.2}$$

We are most interested in finding the s-dependent velocities since it is these that arise from the introduction of time-dependent curvature. We find at $O(s^2)$ that

$$p_{10} = -\tfrac{1}{4}\alpha^3 r\cos\theta\sin t, \tag{5.3}$$

which is just the fluid pressure adjustment to balance the new centrifugal-force terms.

The s-dependent equations are:
continuity

$$u_{10r} + \frac{1}{r}v_{10\theta} + \frac{1}{r}u_{10} = 0, \tag{5.4a}$$

$\boldsymbol{e}_r$

$$\alpha^2 u_{10t} + u_0\,u_{10r} + u_{10}\,u_{0r} + \frac{1}{r}v_0\,u_{10\theta} + \frac{1}{r}v_{10}\,u_{0\theta} - \frac{2}{r}v_0\,v_{10} - \alpha\,\cos\theta\,\cos t\,w_0 = -p_{11r} - \frac{1}{r}\frac{\partial}{\partial\theta}\left[\frac{1}{r}(v_{10} + rv_{10r} - u_{10\theta})\right], \tag{5.4b}$$

$\boldsymbol{e}_\theta$

$$\alpha^2 v_{10t} + u_0\,v_{10r} + u_{10}\,v_{0r} + \frac{1}{r}v_0\,v_{10\theta} + \frac{1}{r}v_{10}\,v_{0\theta} + \frac{1}{r}(u_0\,v_{10} + u_{10}\,v_0) + \alpha\,\sin\theta\,\cos t\,w_0 = -\frac{1}{r}p_{11\theta} + \frac{\partial}{\partial r}\left[\frac{1}{r}(v_{10} + rv_{10r} - u_{10\theta})\right], \tag{5.4c}$$

From (5.4a) we know that there exists a streamfunction ψ_{10} such that $u_{10} = (1/r)\,\psi_{10\theta}, v_{10} = -\psi_{10r}$. Thus (5.4$b$) and (5.4$c$) may be combined to give

$$\alpha^2\nabla^2\psi_{10t} - \alpha\cos t\left(\frac{1}{r}\cos\theta\,w_{0\theta} + \sin\theta\,w_{0r}\right) = \nabla^4\psi_{10} + \frac{1}{r}\left(\psi_{0r}\frac{\partial}{\partial\theta} - \psi_{0\theta}\frac{\partial}{\partial r}\right)\nabla^2\psi_{10} + \frac{1}{r}\left(\psi_{10r}\frac{\partial}{\partial\theta} - \psi_{10\theta}\frac{\partial}{\partial r}\right)\nabla^2\psi_0. \tag{5.5}$$

We are interested in determining the secondary motions generated in the core; however, it is first necessary to determine the behaviour of the flow in the boundary layer, since it is that which drives the secondary motions in the core.

In the viscous boundary layer we take

$$\Psi_{10} = \frac{1}{\alpha}\left(\Psi_{100} + \frac{1}{\alpha}\Psi_{101} + \cdots\right) \tag{5.6}$$

and the boundary layer coordinate is again

$$\eta = \frac{\alpha}{\sqrt{2}}(1 - r). \tag{5.7}$$

The equation for Ψ_{100} is, from (5.5)

$$\tfrac{1}{2}\Psi_{100\eta\eta\eta\eta} - \Psi_{100\eta\eta t} = \sqrt{2}\cos t\,\sin\theta\,W_{00\eta}, \tag{5.8}$$

where $W_{00} = (2R_s)^{1/2}\,(\sin(t + \Phi) + \mathrm{e}^{-\eta}\sin(t + \Phi - \eta))$ (see (2.14)), which has solution

$$\Psi_{100} = \sin\theta\,(2R_s)^{1/2}\left[\tfrac{1}{2}\mathrm{e}^{-\eta}\,\sin\left(2t + \Phi - \eta + \tfrac{1}{4}\pi\right) + \tfrac{1}{2}\mathrm{e}^{-\eta}\,\sin\left(-\Phi + \eta - \tfrac{1}{4}\pi\right) - \frac{1}{2\sqrt{2}}\mathrm{e}^{-\sqrt{2}\eta}\,\sin(2t + \Phi - \sqrt{2}\eta + \tfrac{1}{4}\pi) - \frac{1}{\sqrt{2}}\,\eta\,\cos\Phi + \tfrac{1}{2}\sin(\Phi + \tfrac{1}{4}\pi) + \frac{1}{2\sqrt{2}}\,(1 - \sqrt{2})\sin(2t + \Phi + \tfrac{1}{4}\pi)\right]. \tag{5.9}$$

Ψ_{100} contains time-independent terms, because although $W_{00\eta}$ has no mean part, the product $\cos t\,W_{00\eta}$ does have a mean part. Hence we see that, as $\eta \to \infty$, not only

does Ψ_{100} not tend to zero (displacement effect) but also

$$\Psi_{100\eta} \to -\frac{1}{\sqrt{2}}(2R_s)^{1/2}\cos\Phi\,\sin\theta. \tag{5.10}$$

After an analysis similar to Lyne's the equation for the steady streaming in the core $\psi^{(s)}_{100}$, derived from (5.5), is given by the solution to

$$\nabla^4\psi^{(s)}_{100} + \frac{1}{r}\left(\psi^{(s)}_{00r}\frac{\partial}{\partial\theta} - \psi^{(s)}_{00\theta}\frac{\partial}{\partial r}\right)\nabla^2\psi^{(s)}_{100} + \frac{1}{r}\left(\psi^{(s)}_{100r}\frac{\partial}{\partial\theta} - \psi^{(s)}_{100\theta}\frac{\partial}{\partial r}\right)\nabla^2\psi^{(s)}_{00} = 0, \tag{5.11}$$

subject to the boundary conditions derived from (5.9) and (5.10) that

$$\psi^{(s)}_{100} = 0,\ \ \psi^{(s)}_{100r} = \tfrac{1}{2}(2R_s)^{1/2}\sin\theta\,\cos\Phi \quad \text{on} \quad r = 1. \tag{5.12}$$

(Here $\psi^{(s)}_{00}$ and $\psi^{(s)}_{100}$ are the leading-order steady terms of a power series expansion in α for ψ_0 and ψ_{10}.)

If we make the transformations $\psi_{100} = R_s^{1/2}\chi_{100}$ and $\psi_{00} = R_s\,\chi_{00}$, then the equation to solve is

$$\frac{1}{R_s}\nabla^4\chi_{100} + \frac{1}{r}\left(\chi_{00r}\frac{\partial}{\partial\theta} - \chi_{00\theta}\frac{\partial}{\partial r}\right)\nabla^2\chi_{100} + \frac{1}{r}\left(\chi_{100r}\frac{\partial}{\partial\theta} - \chi_{100\theta}\frac{\partial}{\partial r}\right)\nabla^2\chi_{00} = 0, \tag{5.13}$$

subject to the boundary conditions:

$$\chi_{100} = 0, \quad \chi_{100r} = \tfrac{1}{2}\sqrt{2}\sin\theta\cos\Phi \quad \text{on} \quad r = 1. \tag{5.14}$$

We will clearly be able to solve (5.13) for χ_{100} using the same methods as Lyne (1971) used for (5.1).

5.2. *Analytical streaming solution at small R_s*

Analytic progress towards a solution of (5.1) and (5.13) may be made in the limit of small R_s by considering a small-parameter expansion in powers of R_s (Lyne 1971):

$$\chi_{00} = \chi_{000} + R_s\,\chi_{001} + \cdots, \quad \chi_{100} = \chi_{1000} + R_s\,\chi_{1001} + \cdots. \tag{5.15}$$

The leading-order steady streaming problem (5.1) is reduced to a simple Stokes flow problem, with solution

$$\chi_{00} = -\tfrac{1}{8}\,r(1-r^2)\,\sin\theta - R_s\,\tfrac{1}{3072}\,r^2(1-r^2)^2\,\sin 2\theta + O(R_s^2). \tag{5.16}$$

The steady secondary streaming in the core, to leading order in R_s, proceeds across the tube from the outside of the bend to the inside. This is in the opposite direction to the secondary flow in a pipe when the axial pressure gradient is steady (or when $\alpha \ll 1$ as in the quasi-steady case detailed in § 4). Thus whereas the intuitive idea of 'outwards centrifuging' is valid for steady flow, it is not relevant for oscillatory flow and the apparent 'centrifuging' is negative and thus directed inwards. Lyne verified this analytic result experimentally.

The leading-order solution of (5.13), subject to the boundary conditions (5.14), is

$$\chi_{1000} = -\tfrac{1}{4}\sqrt{2}r\,(1-r^2)\,\sin\theta\,\cos\Phi. \tag{5.17}$$

Thus when $\cos\Phi > 0$ this contribution to the streaming proceeds across the tube from the outside of the bend to the inside (i.e. in the same direction as Lyne's) and thus enhances the streaming arising due to the tube being curved. However, for $\cos\Phi < 0$ the contribution is in the opposite direction, and thus diminishes the streaming. The dependence of the steady streaming on s, given by (5.2), means that

its magnitude will increase with distance from the fixed origin. Of course, since we have considered a small-R_t parameter expansion the effect of this perturbation on the leading-order secondary streaming will be small.

5.3. *Numerical solution at intermediate values of R_s*

In order to determine the behaviour of the secondary streaming in the core at intermediate values of the secondary streaming Reynolds number R_s we must solve equations (5.1) and (5.13) numerically, which we do using a finite difference method. Haddon (1982) has solved Lyne's problem numerically, also using a finite difference method, but with a different iteration procedure.

5.3.1. *Numerical method*

Equations (5.1) and (5.13) must be linearized in order to obtain a system of linear algebraic equations, which can then be solved numerically. This is done using the Newton–Raphson scheme.

Let n label the iteration number, and define ξ_{00}^n as

$$\xi_{00}^n = \chi_{00}^n - \chi_{00}^{n-1}. \tag{5.18}$$

The Newton–Raphson iterative scheme for (5.1) is

$$\nabla^4 \xi_{00}^n + R_s \frac{1}{r}\left(\frac{\partial \chi_{00}^{n-1}}{\partial r}\frac{\partial}{\partial \theta} - \frac{\partial \chi_{00}^{n-1}}{\partial \theta}\frac{\partial}{\partial r}\right)\nabla^2 \xi_{00}^n + R_s \frac{1}{r}\left(\frac{\partial \xi_{00}^n}{\partial r}\frac{\partial}{\partial \theta} - \frac{\partial \xi_{00}^n}{\partial \theta}\frac{\partial}{\partial r}\right)\nabla^2 \chi_{00}^{n-1}$$
$$= -\nabla^4 \chi_{00}^{n-1} - R_s \frac{1}{r}\left(\frac{\partial \chi_{00}^{n-1}}{\partial r}\frac{\partial}{\partial \theta} - \frac{\partial \chi_{00}^{n-1}}{\partial \theta}\frac{\partial}{\partial r}\right)\nabla^2 \chi_{00}^{n-1} \tag{5.19}$$

which is iterated until a converged solution for ξ_{00} is obtained. Similarly, by defining

$$\xi_{100}^n = \chi_{100}^n - \chi_{100}^{n-1}, \tag{5.20}$$

the iteration scheme for equation (5.13) is

$$\nabla^4 \xi_{100}^n + R_s \frac{1}{r}\left(\frac{\partial \chi_{00}^{n-1}}{\partial r}\frac{\partial}{\partial \theta} - \frac{\partial \chi_{00}^{n-1}}{\partial \theta}\frac{\partial}{\partial r}\right)\nabla^2 \xi_{100}^n + R_s \frac{1}{r}\left(\frac{\partial \xi_{100}^n}{\partial r}\frac{\partial}{\partial \theta} - \frac{\partial \xi_{100}^n}{\partial \theta}\frac{\partial}{\partial r}\right)\nabla^2 \chi_{00}^{n-1}$$
$$= -\nabla^4 \chi_{100}^{n-1} - R_s \frac{1}{r}\left(\frac{\partial \chi_{00}^{n-1}}{\partial r}\frac{\partial}{\partial \theta} - \frac{\partial \chi_{00}^{n-1}}{\partial \theta}\frac{\partial}{\partial r}\right)\nabla^2 \chi_{100}^{n-1}$$
$$- R_s \frac{1}{r}\left(\frac{\partial \chi_{100}^{n-1}}{\partial r}\frac{\partial}{\partial \theta} - \frac{\partial \chi_{100}^{n-1}}{\partial \theta}\frac{\partial}{\partial r}\right)\nabla^2 \chi_{00}^{n-1}. \tag{5.21}$$

We wish to solve the flow in the circular plane of cross-section of the pipe. However, since the flow is symmetric about the diameter $\theta = 0, \pi$ we need only compute the flow in one half of the pipe. The computational domain is therefore a semi-circle, polar coordinates (r, θ) are used and grid lines are chosen along lines of constant radius and constant θ.

Both χ and $\partial\chi/\partial r$ are given on $r = 1$ ((5.1) and (5.14)). Since the boundary of the semi-circular domain is a streamline we have that $\chi = 0$ on $\theta = 0, \pi$. We also have zero normal velocity (in the θ-direction) on the line $\theta = 0, \pi$. Thus $\partial u/\partial\theta = (1/r)(\partial^2\chi/\partial\theta^2) = 0$ on $\theta = 0, \pi$.

The governing equations (5.19) and (5.21) are discretized using a second-order-accurate finite-difference technique. A set of linear algebraic equations is obtained, which can be written in matrix form. At each Newton–Raphson iterative step the linear matrix equations are solved using the alternating-direction-implicit (ADI) relaxation

method. In order to make the ADI scheme converge, it is necessary to under-relax, using a relaxation parameter, c, where $0 < c < 1$. The value of c necessary for convergence depends on the size of the mesh used. In general, the finer the mesh, the smaller the value of c required to obtain convergence.

The streamfunction for a given value of R_s is found using the Newton–Raphson method as follows. Suppose ΔR_s is an increment in R_s and χ_L is the solution to the linear problem, $\nabla^4\chi = 0$, corresponding to $R_s = 0$. Then the basic stages of the numerical algorithm are:

(i) Solve the streamfunction equation (5.19), with the corresponding boundary conditions, at $R_s = \Delta R_s$ using $\chi = \chi_L$ as an initial guess to the solution.

(ii) Update R_s to $R_s = 2\Delta R_s$ and solve for the streamfunction using the converged solution for the streamfunction at $R_s = \Delta R_s$ as an initial guess.

(iii) Repeat until the streamfunction at the required value of R_s is obtained.

In order to check the accuracy of the numerical code, we examined the effect of tightening the tolerance criteria for the ADI and Newton–Raphson schemes (ϵ_1 and ϵ_2 respectively) and refining the mesh. To ensure that the chosen tolerances were sufficiently small, we computed the solution at tighter tolerance values and investigated how the obtained numerical solution changed both quantitatively and qualitatively. This was done for a range of values of R_s, but most importantly for the highest value of R_s at which results were obtained ($R_s = 300$) since this case will be the most sensitive. For $R_s = 300$, initially we took $\epsilon_1 = \epsilon_2 = 10^{-5}$. We then computed the solutions at $\epsilon_1 = \epsilon_2 = 10^{-6}$. It was found that the maximum difference between the values of $\psi_{i,j}$ obtained at the two different tolerances was $O(10^{-5})$, and the qualitative behaviour of the obtained solutions was unchanged.

The effect of grid-refinement on the numerical solution was also investigated. Initially, the solutions at various R_s were calculated on the coarsest mesh possible that allowed a convergent solution to be found (as the value of R_s increases, it is necessary to refine the mesh in order to converge to a solution.) For example, for values of R_s up to about 170, solutions were obtained using a (21×21) grid, whereas for values of R_s between 170 and 300, solutions were obtained on a (31×31) mesh. For $R_s = 10$ and $R_s = 50$, we also calculated the solution on grids of (41×41) and (81×81). For $R_s = 10$, the maximum difference between the solutions found on a (21×21) and a (41×41) grid was order 10^{-4} and on a (41×41) and (81×81) grid was order 10^{-5}. For $R_s = 50$ the difference was $O(10^{-4})$. Grid refinements were also carried out for $R_s = 100$ where again the differences were $O(10^{-4})$. For $R_s = 200$ and 300 it was found that the differences were $O(10^{-5})$. Hence the underlying physics of the system was captured using the computationally less expensive coarser mesh.

We looked at the effect of tightening the tolerances and refining the mesh on the maximum value of vorticity, ω, that is obtained. Since vorticity involves second-order derivatives, $\omega = -\nabla^2\psi$, it is a good quantity to consider, since it is likely to be the most poorly behaved of the system. It was found that making the tolerances tighter had a small effect on the maximum value of vorticity obtained. For example, for $R_s = 10$, the difference between solutions obtained at the tolerances $\epsilon_1 = \epsilon_2 = 10^{-6}$ and $\epsilon_1 = \epsilon_2 = 10^{-7}$ was 0.04%. For $R_s = 300$, the difference between solutions obtained at $\epsilon_1 = \epsilon_2 = 10^{-5}$ and $\epsilon_1 = \epsilon_2 = 10^{-6}$ was 0.3%.

Also, for $R_s = 10$, halving the mesh size resulted in a 0.02% change in the value of the maximum vorticity. For $R_s = 50$, halving the mesh size resulted in a 0.1% change in the maximum value of the vorticity. For $R_s = 100$, the change was again 0.1%. As the value of R_s increased, however, the percentage change also increased. For $R_s = 200$, it was found that refining the mesh resulted in a 6% change and for

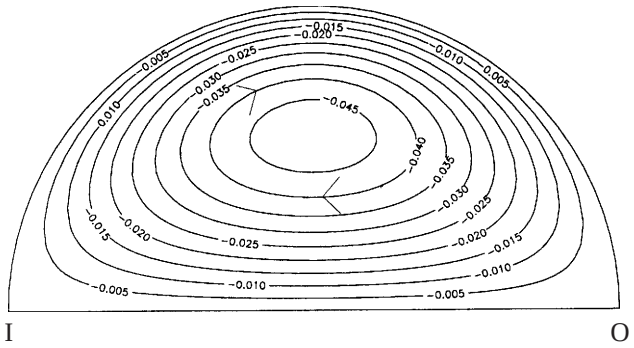

FIGURE 3. Secondary streamfunction, χ_{00}, for $R_s = 0$.

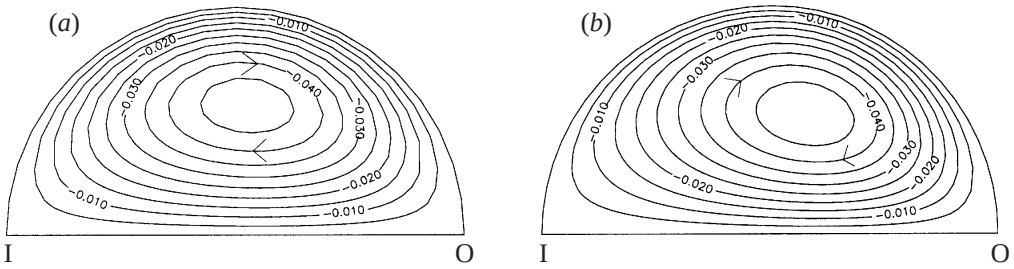

FIGURE 4. Numerical solution for the streamfunction, χ_{00}, for increasing R_s: (*a*) $R_s = 50$; (*b*) $R_s = 250$.

$R_s = 300$, the change was 8%. The computational scheme would clearly have to be refined if we were to go to higher values of R_s.

5.3.2. *Results*

The leading-order secondary streamfunction, χ_{00}, at $R_s = 0$ is shown in figure 3. The streamfunction is symmetric about the line $\theta = \pi/2$. Figure 4 shows how the flow develops with increasing secondary streaming Reynolds number, R_s. The secondary streaming still proceeds across the centre of the tube from the outside of the bend towards the inside. As the value of R_s increases, the advection terms in (5.1) become increasingly important, and it is these effects that we observe here. Figure 4(*a*) shows the secondary streamlines when $R_s = 50$. The stationary point, or vortex centre, is shifted in the direction of the driving secondary flow, towards the outer wall of the pipe. As the value of R_s increases to $R_s = 250$, the vortex centre continues to be shifted in the direction of the flow (figure 4*b*).

We note that the solutions for the secondary streamfunction, χ_{00}, at $R_s = 50$ and $R_s = 250$ look similar (figure 4*a*, *b*). As R_s increases, however, there is a definite change in the streamfunction solution which may be clearly seen by considering the difference between the solutions at various R_s. Figure 5(*a*) shows the difference between the streamfunction values corresponding to $R_s = 50$ and $R_s = 10$. The convective motion consists approximately of two counter-rotating eddies. This is consistent with the analytic solution found at small values of R_s, which gives the first correction to the viscous Stokes layer solution to be proportional to $\sin 2\theta$. As the value of R_s increases, the convective motion still has the form of two counter-rotating eddies, but now they are no longer symmetrical and, moreover, are of unequal size (figure 5*b*).

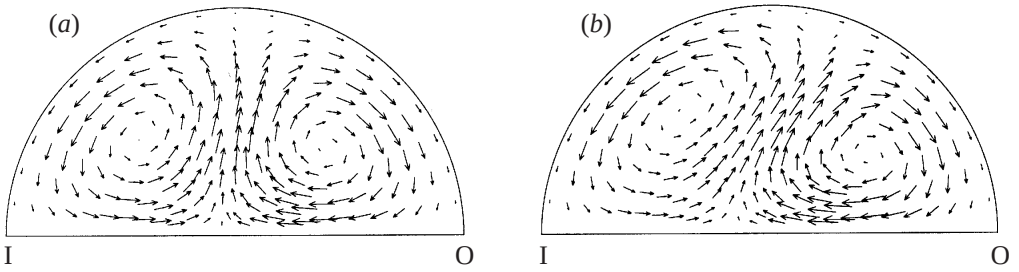

FIGURE 5. Difference between the secondary streamfunction solutions at: (*a*) $R_s = 50$ and $R_s = 10$; (*b*) $R_s = 250$ and $R_s = 10$.

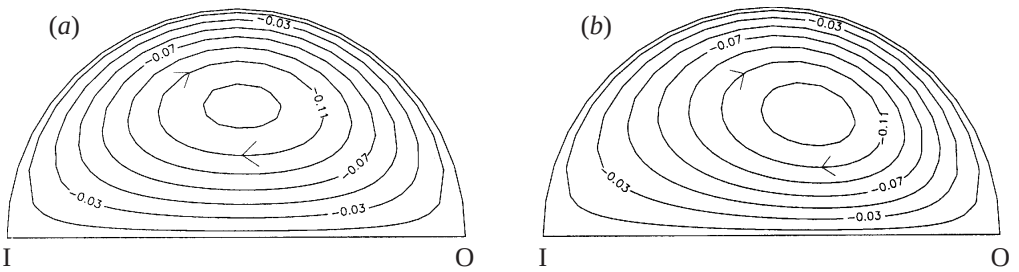

FIGURE 6. Numerical solution for the secondary streamfunction perturbation, χ_{100}, for increasing R_s. Results are presented for $\cos\Phi = 1$: (*a*) $R_s = 10$; (*b*) $R_s = 100$.

Next we consider the perturbation to the secondary streaming that arises due to the introduction of time-dependent curvature. We present results for the secondary streamfunction, χ_{100}, at values of $R_s = 10$ and 100 (figure 6*a*, *b*).

The interesting feature here is that the direction of the perturbation to the steady secondary flow is dependent on the phase difference, Φ, between the oscillatory pressure gradient and the time-dependent curvature. When $\cos\Phi$ is positive, the perturbation to the secondary flow is in the same direction as for Lyne. When $\cos\Phi$ is negative the reverse is true. The results presented in figure 6(*a*, *b*) are for $\cos\Phi = 1$.

At this order the advection effects are stronger. Whereas in (5.1) we saw that the streamfunction χ_{00} was advected by itself, here the streamfunction χ_{100} is advected by χ_{00} and χ_{00} is advected by χ_{100} (see equation (5.13)). Thus the advective effects are doubled, and this is reflected in the greater value of the streamfunction χ_{100} for a given value of R_s, and the greater advection of the vorticity for a given value of R_s.

The direction in which the vortex centre of the secondary streamlines is 'skewed' is independent of the sign of $\cos\Phi$. It is always towards the outside wall for the range of secondary streaming Reynolds numbers that we consider here. Thus, when $\cos\Phi$ is negative, we have the interesting situation that the direction of skewing of the stagnation point of the secondary streamlines is in the opposite direction to the driving circumferential velocity. When $\cos\Phi = 0$, χ_{100} is identically zero and there is no contribution to the steady secondary streamfunction at this order.

The dependence of χ_{100} on s means that the magnitude of the perturbation to the streamfunction will increase with distance from the fixed origin.

5.4. *Solution at asymptotically large values of* R_s

At large values of R_s it is hypothesized that the effect of viscosity is confined to boundary layers of thickness $R_s^{-1/2}$ near $r = 1$. These come together at $\theta = 0$ and

erupt across the centre of the tube. Lyne (1971) postulated a scheme in which the wall boundary layers are supplemented by a layer of thickness $R_s^{-1/2}$ across the plane of symmetry, the bulk of the core flow being inviscid. In the inviscid region the streamlines are closed, and therefore the vorticity is uniform and of opposite sign in the two regions (Batchelor 1956); one reason why the shear layer across the middle of the tube is required is to smooth out the discontinuity in vorticity between the two inviscid regions.

Haddon (1982) gave a numerical solution of Lyne's (1971) steady streaming problem (equation (5.1) above) which he took to large values of R_s (up to 3000). He was able to show that the vorticity distribution in one half of the pipe cross-section (along $r = 1/2,\ 0 < \theta < \pi$, and along $\theta = \pi/2\ ,\ 0 < r < 1$) became approximately uniform over a substantial part of the region. Moreover, the value of the vorticity, in the limit as $R_s \to \infty$ and the mesh size $\to 0$, was (to two significant figures) equal to -0.56, precisely the value predicted independently by Lyne. We did not take our numerical results to a high enough value of R_s to achieve this limit, although the leading-order vorticity profile along $\theta = 3\pi/2$ did tend to flatten out near $r = 1/2$ at the larger values of R_s. The large-R_s solution to the perturbation problem (5.13)–(5.14) has not been obtained.

6. Physiological application

In the context of blood flow in the coronary arteries, relevant parameter values are (to one significant figure)

$$\begin{aligned} &\text{kinematic viscosity of blood} && \nu = 4 \times 10^{-6}\,\mathrm{m^2\,s^{-1}}\ , \\ &\text{period of the heart beat} && T \approx 1\,\mathrm{s}. \end{aligned}$$

We consider those extramyocardial arteries whose curvature is single-signed and varies relatively slowly with longitudinal position. For such arteries we may take (Guyton 1986)

$$\begin{aligned} &\text{radius} && a = 2 \times 10^{-3}\,\mathrm{m}, \\ &\text{radius of curvature} && \hat{R} = 3 \times 10^{-2}\,\mathrm{m}, \\ &\text{peak time–averaged blood velocity} && U_p = 3 \times 10^{-1}\,\mathrm{m\ s^{-1}}, \\ &\text{velocity amplitude} && \hat{W}_p = 2 \times 10^{-1}\,\mathrm{m\ s^{-1}}; \end{aligned}$$

moreover, if we assume that the volume of the left ventricle is halved during systole, then the radius of curvature will be reduced by a factor $2^{-1/3} \approx 8 \times 10^{-1}$. From this, we find

$$\delta_0 = a/\hat{R} \approx 0.07, \quad \epsilon \approx 0.1. \tag{6.1}$$

Also

$$Re = \frac{U_p\, a}{\nu} \approx 150, \quad \alpha^2 = \frac{a^2}{\nu T} \approx 1. \tag{6.2}$$

We considered a dimensionless oscillatory pressure gradient:

$$-p_s = \alpha^2\, W_p \cos(t + \Phi), \tag{6.3}$$

where W_p is the dimensionless velocity amplitude that would be driven by such a pressure gradient in a straight pipe containing an inviscid fluid. Here the velocities were non-dimensionalized with respect to ν/a and so

$$W_p = a\hat{W}_p/\nu \approx 100. \tag{6.4}$$

The secondary streaming Reynolds numbers, R_s and R_{s_1}, are defined as

$$2R_s = \frac{(2\delta_0)\,W_p^2}{\alpha^2} = \frac{(2\delta_0)}{\alpha^2}\left(\frac{a\hat{W}_p}{\nu}\right)^2,$$

$$R_{s_1} = (2\delta_0)\,\epsilon W_p = (2\delta_0)\,\epsilon\left(\frac{a\hat{W}_p}{\nu}\right) \tag{6.5}$$

(cf. (2.32)) and so

$$2R_s \approx 1320, \quad (2R_s)^{1/2} \approx 36, \quad R_{s_1} \approx 1.4. \tag{6.6}$$

The parameter R_t, (2.33), is

$$R_t = \alpha\epsilon \approx 0.1. \tag{6.7}$$

When considering the flow driven by an oscillatory pressure gradient, the curvature was assumed to be small ($\delta_0 \ll 1$) and to vary by a relatively small amount ($\epsilon \ll 1$), assumptions that are reasonably well satisfied in the coronary arteries.

Initially α and R_s were kept order one compared with δ_0 and R_t. A small-parameter expansion was carried out in powers of δ_0 followed by a small-parameter expansion in powers of R_t, so that we assumed that $\delta_0 \ll R_t$. The equations were then solved for asymptotically large and small values of the frequency parameter, α.

From (6.2), (6.6) and (6.7), the assumption that α and R_s are order one compared with δ_0 and R_t is reasonably well satisfied. Moreover, although δ_0 is not much smaller than R_t, it is smaller. The assumptions that $\alpha \ll R_s$ (low-frequency case) and $R_t \ll 1/\alpha^2$ (high-frequency case) are approximately satisfied; however $\alpha \approx 1$ and so is neither large nor small. In § 5 results were found for small and intermediate values of R_s. From (6.6) we see that the most physiologically significant solutions correspond to those found numerically for intermediate values of R_s.

It appears that at present, the small-α case is most applicable to flow in the coronary arteries. For the small-α case, the magnitude of the ratio between the first perturbation to the time-dependent axial wall shear stress, due to the introduction of time-dependent curvature, (4.13), and the leading-order time-dependent axial wall shear stress (4.3) is, with $s = O(1)$, approximately 8×10^{-4}. The corresponding ratio between the azimuthal wall shear stress perturbation (4.14) and the leading-order azimuthal wall shear stress (4.6) is 1×10^{-2}. Thus the predicted effect, for this particular range of parameters, is rather small. Our results are more significant for the light they shed on the qualitative effect of the time-dependent curvature on the distribution of wall shear stress. It was found that the Coriolis force terms, introduced into the equations by the time-dependent curvature, led to the generation of a steady secondary streaming perturbation. For low frequency, this steady streaming was towards the outside of the bend when the phase difference, Φ, between the curvature and the axial pressure gradient was such that $\cos\Phi > 0$ (the opposite being true when $\cos\Phi < 0$). This perturbation to the steady streaming resulted in a correction to the axial velocity profile, with corresponding perturbations to the axial wall shear stress.

During systole, the increased intramyocardial pressure resulting from the contraction of the thick-walled left ventricle hinders blood flow into the heart muscle (but does facilitate venous drainage by compressing the coronary sinus and other veins). When diastole begins, the rate of flow rapidly increases to reach a maximum level in early diastole, from which it gradually declines. Now, when the ventricle contracts, the rotation of the artery is negative, and so $\cos t > 0$. The phase, Φ, must be such that the driving oscillatory pressure gradient rises initially and then starts to fall, as

the flow of blood is hindered by the increased intramyocardial pressure. At the start of diastole, the rotation of the artery is positive, so that $\cos t < 0$, and the phase difference, Φ, must be such that the driving pressure gradient rises rapidly and then gradually decreases. For this to be true, it is necessary that $\pi/2 < \Phi < \pi$, so that $\cos \Phi < 0$. Thus for small α, we see that there is an increase in wall shear stress on the inside wall, which may be protective against atherosclerosis, and a decrease on the outside wall. Since atherosclerosis is more often found on the inside of the curve, this suggests that the prevalence of atherosclerosis would be worse without movement of the artery.

The authors would like to thank Dr D. G. Lynch for his contribution to the derivation of the equations. The work was performed in the Department of Applied Mathematical Studies, University of Leeds. The award of a Mathematical Biology Research Studentship to S.L.W. by the Wellcome Trust is gratefully acknowledged. Final preparation of this manuscript was done while S. L. W. was a Research Associate with Professor J. B. Grotberg at the Biomedical Engineering Dept., Northwestern University, Evanston, IL 60208, USA.

REFERENCES

Batchelor, G. K. 1956 On steady laminar flow with closed streamlines at large Reynolds number. *J. Fluid Mech.* **1**, 177–190.

Berger, S. A., Talbot, L. & Yao, L. S. 1983 Flow in curved pipes. *Ann. Rev. Fluid Mech.* **15**, 461–512.

Blennerhassett, P. 1976 Secondary motion and diffusion in unsteady flow in a curved pipe. PhD Thesis, Imperial College, London.

Caro, C. G., FitzGerald, J. M. & Schroter, M. F. 1971 Atheroma and arterial wall shear: observation, correlation and proposal of a shear dependent mass transfer mechanism for atherogenesis. *Proc. R. Soc. Lond.* B **177**, 109–159.

Chandran, K. B. & Yearwood, T. L. 1981 An experimental study of physiological pulsatile flow in a curved tube. *J. Fluid Mech.* **111**, 59–85.

Chandran, K. B., Yearwood, T. L. & Wieting, D. M. 1979 An experimental study of pulsatile flow in a curved tube. *J. Biomech.* **12**, 793–805.

Dean, W. R. 1927 Note on the motion of fluid in a curved pipe. *Phil. Mag.* **20**, 208–223.

Dean, W. R. 1928 The streamline motion of fluid in a curved pipe. *Phil. Mag.* (7) **5**, 673–695.

Friedman, M. H. 1993 Arteriosclerosis research using vascular flow models: from 2D branches to compliant replicas. *J. Biomech. Engng* **115**, 595–601.

Giddens, D. P., Zarins, C. K. & Glagov, S. 1993 The role of fluid mechanics in the localization and detection of Atherosclerosis. *J. Biomech. Engng* **115**, 588–594.

Guyton, A. C. 1986 *Textbook of Medical Physiology*. Saunders.

Haddon, E. W. 1982 A high Reynolds number flow with closed streamlines. *8th Intl Conf. on Numerical Methods in Fluid Dynamics. Aachen.* Lecture Notes in Physics, Vol. 170, pp. 233–238 Springer.

Hamakiotes, C. C. & Berger, S. A. 1990 Periodic flows through curved tubes: the effect of the frequency parameter. *J. Fluid Mech.* **210**, 353–370.

Ku, D. N., Giddens, D. P., Zarins, C. K. & Glagov, S. 1985 Pulsatile flow and atherosclerosis in the human carotid bifurcation: positive correlation between plaque location and low and oscillating shear stress. *Arteriosclerosis* **5**, 293–302.

Lin, J. J. & Tarbell, J. M. 1980 An experimental and numerical study of periodic flow in a curved tube. *J. Fluid Mech.* **100**, 623–638.

Lynch, D. G., Waters, S. L. & Pedley, T. J. 1996 Flow in a tube with non-uniform, time-dependent curvature: governing equations and simple examples. *J. Fluid Mech.* **323**, 237–265.

Lyne, W. H. 1971 Unsteady viscous flow in a curved pipe. *J. Fluid Mech.* **45**, 13–31.

Mullin, T. & Greated, C. A. 1980*a* Oscillatory flow in curved pipes. Part I. The developing-flow case. *J. Fluid Mech.* **98**, 383–395.

Mullin, T. & Greated, C. A. 1980*b* Oscillatory flow in curved pipes. Part II. The fully-developed case. *J. Fluid Mech.* **98**, 397–416.

Pedley, T. J. 1980 *The Fluid Mechanics of Large Blood Vessels.* Cambridge University Press.

Rabadi, N. J., Simon, H. A. & Chow J. C. F. 1980 Numerical solution for fully developed, laminar pulsating flow in curved tubes. *Numer. Heat Transfer* **3**, 225–239.

Riley, N. 1981 High-Reynolds number flows with closed streamlines. *J. Engng Maths* **15**, 15–27.

Singh, M. P. 1974 Entry flow in a curved pipe. *J. Fluid. Mech.* **65**, 517–539.

Smith, F. T. 1975 Pulsatile flow in curved pipes. *J. Fluid Mech.* **71**, 15–42.

Smith, F. T. 1976 Steady motion within a curved pipe. *Proc. R. Soc. Lond.* A **347**, 345–370.

Talbot, L. & Gong, K. O. 1983 Pulsatile entry flow in a curved pipe. *J. Fluid Mech.* **127**, 1–25.

Waters, S. L. 1996 Coronary artery haemodynamics: pulsatile fluid flow in a tube of time-dependent curvature. PhD thesis, University of Leeds.

Yao, L.-S. & Berger, S. A. 1975 Entry flow in a curved pipe. *J. Fluid Mech.* **67**, 177–196.

Zalosh, R. G. & Nelson, W. G. 1973 Pulsating flow in a curved tube. *J. Fluid Mech.* **59**, 693–705.